VTT Technical Research Centre of Finland

Deuterium and helium outgassing following plasma discharges in WEST

Bisson, R.; Hodille, E. A.; Gaspar, J.; Douai, D.; Wauters, T.; Gallo, A.; Gunn, J.; Hakola, Antti; Loarer, T.; Nouailletas, R.; Morales, J.; Pégourié, B.; Reux, C.; Sabot, R.; Tsitrone, E.; Vartanian, S.; Wang, E.; Fedorczak, N.; Brezinsek, S.; WEST Team

Published in:
Nuclear Materials and Energy

DOI:
10.1016/j.nme.2020.100885

Published: 01/03/2021

Document Version
Publisher's final version

Nuclear Materials and Energy 26 (2021) 100885

Contents lists available at ScienceDirect

Nuclear Materials and Energy

journal homepage: www.elsevier.com/locate/nme

Deuterium and helium outgassing following plasma discharges in WEST: Delayed D outgassing during D-to-He changeover experiments studied with threshold ionization mass spectrometry

R. Bisson [a,*], E.A. Hodille [b], J. Gaspar [c], D. Douai [b], T. Wauters [d], A. Gallo [a], J. Gunn [b], A. Hakola [e], T. Loarer [b], R. Nouailletas [b], J. Morales [b], B. Pégourié [b], C. Reux [b], R. Sabot [b], E. Tsitrone [b], S. Vartanian [b], E. Wang [f], N. Fedorczak [b], S. Brezinsek [f], WEST team[1]

[a] Aix-Marseille Univ, CNRS, PIIM, UMR 7345, Marseille F-13397, France
[b] IRFM, CEA-Cadarache, F-13108 Saint-Paul-lez-Durance, France
[c] Aix-Marseille Univ, IUSTI, Marseille F-13397, France
[d] LPP-ERM/KMS, EUROfusion Consortium Member, TEC, Brussels, Belgium
[e] VTT, P.O. Box 1000, FI-02044 VTT, Finland
[f] Forschungszentrum Jülich GmbH, Institut für Energie- und Klimaforschung plasmaphysik, D-52425 Jülich, Germany

ARTICLE INFO

Keywords:
Tokamak
Gas balance
Helium
Deuterium
Outgassing
Desorption
Tungsten
Plasma facing components
Macroscopic rate equation modeling

ABSTRACT

Threshold ionization mass spectrometry (TIMS) is one of two methods envisioned in ITER to quantify the helium (He) fusion product in the exhaust pumping lines during plasma discharges. We present the first demonstration of another potential application of TIMS in a tokamak environment, namely, the analysis of deuterium (D) and He outgassing following a plasma discharge i.e. during the post-discharge. This method has been tested with sub-second temporal resolution in WEST during its first He plasma discharges in the so-called He changeover experimental campaign. The calibration method of TIMS using a D plasma discharge is presented while the uncertainties related to TIMS during rapid pressure variations, i.e. upon plasma breakdown and plasma termination, are discussed. The first results obtained with TIMS during consecutive D and He plasma discharges in the full tungsten (W) tokamak WEST are reported. It is found that the time evolutions for He and D outgassing in the post-discharge are markedly different. On one hand, He outgassing is instantaneous and decays within 60 s until the He signal gets below detection level. On the other hand, D outgassing can reach a maximum up to several tens of seconds after the termination of the plasma and this outgassing can last for about 10 min. These striking differences should be related to different retention and outgassing from WEST plasma facing components, presently constituted of actively-cooled ITER-like W units and inertially cooled W-coated graphite. Potential mechanisms at the origin of the different outgassing behavior for D and He in W plasma facing components are discussed in light of a systematic analysis of the He and D gas balance and a macroscopic rate equation modeling of the D outgassing from the divertor strike points.

1. Introduction

ITER aims to operate a self-sustained deuterium/tritium (D/T) "burning plasma" with a divertor magnetic configuration dedicated to exhaust the ionized fusion product (helium, He) such that its concentration in the confined plasma remains sufficiently low to avoid fuel mixture dilution [1]. During a plasma discharge, He quantification in ITER exhaust pumping lines is foreseen. In this context, two methods are envisaged in ITER for this He quantification; one based on optical Penning gauge spectroscopy [2] and the other one based on threshold ionization mass spectrometry (TIMS). The latter is used in the reported analysis and is rather widely investigated in other devices [2–7]. Additionally, in the current planning of the ITER operational phases, it is intended to perform He plasma discharges to demonstrate high confinement mode without nuclear activation of the vacuum vessel components [1]. However, there are some concerns about the evolution

* Corresponding author.
E-mail address: regis.bisson@univ-amu.fr (R. Bisson).
[1] See http://west.cea.fr/WESTteam.

https://doi.org/10.1016/j.nme.2020.100885
Received 31 July 2020; Received in revised form 9 November 2020; Accepted 8 December 2020
Available online 14 December 2020

of the performance of the tungsten (W) divertor under intense He flux, from both the thermomechanical [8,9] and the He/D/T retention and outgassing perspectives [10,11]. Helium is not soluble in W and morphology changes can be expected when exposed to high He fluxes associated with high surface temperatures (T_{surf}). Indeed, He can form nanobubbles in the T_{surf} range of 600–700 K, fuzz as T_{surf} reaches 900 to 1900 K and create large voids as T_{surf} gets larger than 2000 K [12].

To address these issues, WEST, the steady-state tokamak dedicated to testing the actively-cooled ITER-like W divertor technology [13,14], ran its first "pure" He plasma experimental campaign. Actively-cooled ITER-like W units and inertially-cooled W-coated graphite plasma facing components, previously exposed to D plasmas, were exposed for the first time to a large number of He plasma discharges in the so-called He changeover campaign. TIMS was used to perform D and He particle balance analysis both during the discharge and in the post-discharge phase. In this contribution, we focus on the post-discharge particle balance.

Initially discussed by Coyne *et al.* [3] for the JET tokamak, with carbon-dominated plasma facing components which generate various hydrogenated and deuterated hydrocarbons, TIMS allows discriminating in a quadrupole mass spectrometer (QMS) a couple of ionic species with similar mass-over-charge (m/z) ratio thanks to their difference of ionization threshold. For the "burning D/T plasma" in ITER, important ions are D_2^+ and He^+. These two species of $m/z \cong 4$ are apart by about 0.02 amu making their m/z separation possible only in dedicated high-end QMS systems. However, the ionization threshold of D_2 is ~15.5 eV while the one of He is ~24.6 eV [15]. Thus, selective detection of D_2 and He is possible if the kinetic energy of the ionizing electrons can be varied below and above 25 eV, which is the case for most of recent common QMS (also known as residual gas analyzers – RGAs). Quantification of He and D_2 within a binary mixture is possible thanks to a dedicated calibration method which accounts for practical aspects beyond the difference of the ionization cross sections of the two species. The calibration method used so far [2,5] consists in setting successive pure D_2 constant pressures (so-called plateaus) and in determining the function that links the D_2 signal at two electron energies across the ionization threshold of He. Such calibration allowed recent laboratory experiments to evaluate He and D retention following simultaneous or sequential implantations of D and He ions in W samples with Temperature Programmed Desorption [11,16]. To the best of our knowledge, EAST has been the first tokamak to use such calibrated TIMS detection to monitor the evolution of D_2 outgassing during He plasma cleaning of plasma facing components [5] with a time resolution of ~10 s.

In this paper, we present another application of TIMS allowing for the simultaneous analysis of D and He outgassing from a tokamak plasma discharge with sub-second temporal resolution. In section 2.1, we present the He changeover experimental campaign in WEST. In section 2.2, we describe a new TIMS calibration method allowing for the analysis of the variation of the D/He gas balance concomitant with the pressure variation occurring in the discharge and after its termination i.e. in the post-discharge. In section 2.3, we stress the importance of having a gas tracer (here the HD isotopologue) in order to correct for QMS sensitivity drifts within an experimental campaign. In section 3.1, we estimate the precision and limitation of TIMS during the plasma discharge and in the post-discharge. In section 3.2, we present the first observation of different outgassing behaviors for He and D in W plasma facing components, a feature only possible because of the time resolution achieved presently. In section 3.3, we analyze the gas balance evolution during the WEST He changeover campaign and compare it with a macroscopic rate equation model describing D outgassing from the divertor strike points. This way we pinpoint the most likely mechanisms at the origin of the different outgassing behavior for He and D and we suggest further experimental studies in WEST.

2. Methods

2.1. He changeover campaign in WEST

The first D-to-He and He-to-D changeover experiments in WEST have been carried out over 200 discharges cumulating up to 975 s of He plasma. The main plasma parameters were a plasma current ranging from 0.5 to 0.7 MA, a toroidal magnetic field of 3.7 T, a lower single null magnetic configuration from ohmic to auxiliary heating by the lower hybrid (LH) system up to 3.0 MW and discharge durations up to 20 s (discharge number #55326). The reported experiments have been performed over three experimental days, starting with a device fully commissioned in D and moved to "pure" He plasmas (26 He discharges from #55243 to #55269) followed by 4 hours of He glow discharges conditioning (GDC) during the night. The second day (#55270 to #55302) started in He, followed by a changeover from He-to-D and D-to-He (#55288 to #55297 in D) while He GDC were once again applied during the night prior to the last experimental day. The final session comprised 23 discharges in He.

The associated TIMS measurements of the He and D gas balance were performed with a QMS manufactured by Hiden Analytical (DLS-1) and installed in the outer mid-plane in the main pumping port of the tokamak vessel. The QMS is equipped with two ionization filaments (for improved productivity) and only one is used at all times. The electron energy resolution of this QMS was 0.5 eV with a sampling rate below 100 ms. For the present campaign, eight m/z channels were recorded. The first three channels were dedicated to the detection of the three hydrogen isotopologues H_2, HD and D_2 at $m/z = 2, 3$ and 4, respectively, using an electron energy of 23 eV. The next three channels were dedicated to the detection of the three hydrogen isotopologues and He using the same m/z but with an electron energy of 50 eV. Additionally, $m/z = 6$ was selected to control the presence of D_3^+ and $m/z = 28$ was measured to check for the presence of N_2, as it was used occasionally in the early plasma phase (0–3 s) to ease the plasma formation. These 8 channels were measured every 685 ms.

Fig. 1 shows the raw QMS data of the reference D plasma discharge #55242. This discharge is the last one performed in WEST with plasma facing components virgin of any He exposure. One can see the expected abundancy of hydrogen isotopologues in a D operated tokamak with $D_2 > HD > H_2$. Although N_2 has been injected (0.62 $Pa.m^3$) in the early phase of this plasma, no trace of N_2 was detected in the discharge or in

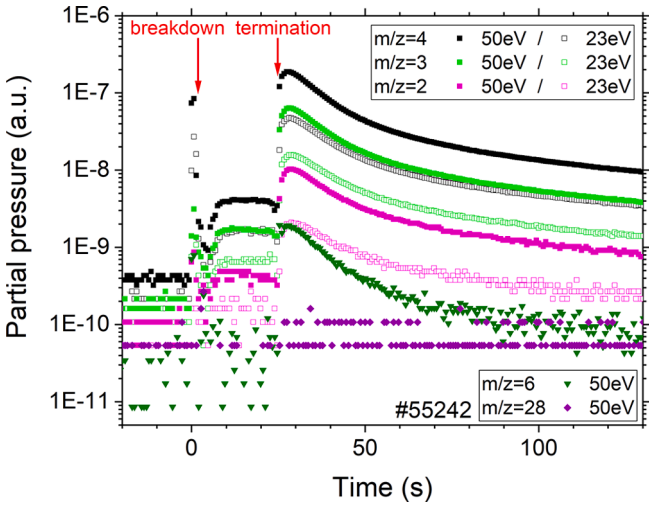

Fig. 1. Raw QMS data employing two electron ionization energies for TIMS measurements during the reference D discharge #55242. The plasma discharge is delimited by its breakdown and its termination. The post-discharge is defined after plasma termination. Eight channels are employed to record every 685 ms the following species: H_2, HD, D_2, He, D_3^+ and N_2/CO.

the post-discharge i.e. injected nitrogen was trapped in plasma facing components [17]. One can detect a significant signal for D_3^+ in the post-discharge, consistent with the pressure in the pumping duct where the QMS is located.

2.2. TIMS calibration using a deuterium reference discharge

As explained in the introduction, the calibration of TIMS is realized by determining the function that transforms the QMS signal for D_2 below the ionization threshold of He into the D_2 signal above the He threshold. Fig. 2a shows how this calibration is realized during the reference D discharge #55242: one plots the ratio of $m/z = 4$ signals recorded at 50 eV and 23 eV electron energies as a function of the D_2 signal at 23 eV, the obtained curve being used to adjust the calibration function $F^{50/23}_{m/z=4}$. This reference "pure" D discharge has been used to calibrate the QMS response to the D_2 species since the pressure variation during the plasma breakdown, the plasma discharge and the post-discharge conveniently sweep the pressure range in which the QMS will be used in the He changeover campaign. It is found that the value of $F^{50/23}_{m/z=4}$, initially of the order of the expected ionization cross section ratio for D_2 of 2.1 [15], increases up to a value of 4 along the two-to-three orders of magnitude excursion of the QMS signals at $m/z = 4$. Thus, $F^{50/23}_{m/z=4}$ is not a constant function but instead a non-linear function. This is in contrast with laboratory D_2 calibration experiments performed below 10^{-4} Pa [11] but in agreement with tokamak calibration experiments performed with D_2 plateaus to higher pressures [5].

We account for the non-linearity of the QMS response with pressure by using a non-linear function adjustment of $F^{50/23}_{m/z=4}$ (Fig. 2a). With this adjustment, the contribution from He species on the QMS signal at $m/z = 4$ as well as the He partial pressure can be evaluated. The evaluation of the He partial pressure P_{He} is made with the following equation

$$P_{He} = \left[P^{50eV}_{m/z=4} - \left(P^{23eV}_{m/z=4} \times F^{50/23}_{m/z=4}\right)\right] \times \frac{\sigma^{50eV}_{D_2}}{\sigma^{50eV}_{He}}$$

with $P^{50eV}_{m/z=4}$ the raw $m/z = 4$ signal measured at 50 eV and $\left(P^{23eV}_{m/z=4} \times F^{50/23}_{m/z=4}\right)$ the evaluation of the D_2 signal contributing to the $m/z = 4$ signal measured at 50 eV. Thus, the term in brackets is the evaluation of the He signal contributing to the $m/z = 4$ at 50 eV. The multiplying factor $\frac{\sigma^{50eV}_{D_2}}{\sigma^{50eV}_{He}}$ is the ratio of ionization cross sections at 50 eV electron energy for D_2 and He [15]. It allows to correct for the different gauge sensitivity of the two species and thus it transforms the term in brackets into a He partial pressure that can be quantitatively compared to the D_2 partial pressure, defined as

$$P_{D_2} = P^{23eV}_{m/z=4} \times F^{50/23}_{m/z=4}$$

and to the HD partial pressure simply determined with

$$P_{HD} = P^{50eV}_{m/z=3}$$

where $P^{50eV}_{m/z=3}$ is the raw $m/z = 3$ signal measured at 50 eV.

Then, we define the He balance as

$$\frac{He}{He + D} = \frac{P_{He}}{P_{He} + P_{HD} + 2 \times P_{D_2}}$$

and finally the D balance as

$$\frac{D}{He + D} = \frac{P_{HD} + 2 \times P_{D_2}}{P_{He} + P_{HD} + 2 \times P_{D_2}}$$

Using this methodology on the D reference discharge #55242, we find that D contributes to $100 \pm 1\%$ of the outgassing balance, consistent with the fact that this discharge is performed on plasma facing components that have never been exposed to He flux.

We checked the consistency of our calibration procedure for the evaluation of D_2 from $m/z = 4$ at 50 eV by applying it to the $m/z = 3$ signal related to HD. For the D reference discharge #55242, we found that the measured $m/z = 3$ signal at 50 eV can be reproduced from the $m/z = 3$ signal at 23 eV using the calibration function $F^{50/23}_{m/z=4}$ only if a constant multiplication factor (1.17, here) is applied, i.e. $F^{50/23}_{m/z=3} \cong 1.17 \times F^{50/23}_{m/z=4}$. The need for a constant multiplication factor translates the fact that the two calibration functions are not superimposed but are parallel to each other when defined as a function of partial pressure (Fig. 2a). A difference of 17% between $F^{50/23}_{m/z=3}$ and $F^{50/23}_{m/z=4}$ cannot be related to an isotopic effect in ionization cross sections since it has been measured to be smaller than 3% for H_2 and D_2 [18]. Instead, we found that the origin of this 17% difference in calibration functions is related to the way we define them i.e. as a function of partial pressures. Indeed, it is the total pressure during the D reference discharge that truly determines the pressure evolution of the calibration functions, as demonstrated in Fig. 2b, not the partial pressure. This observation suggests that

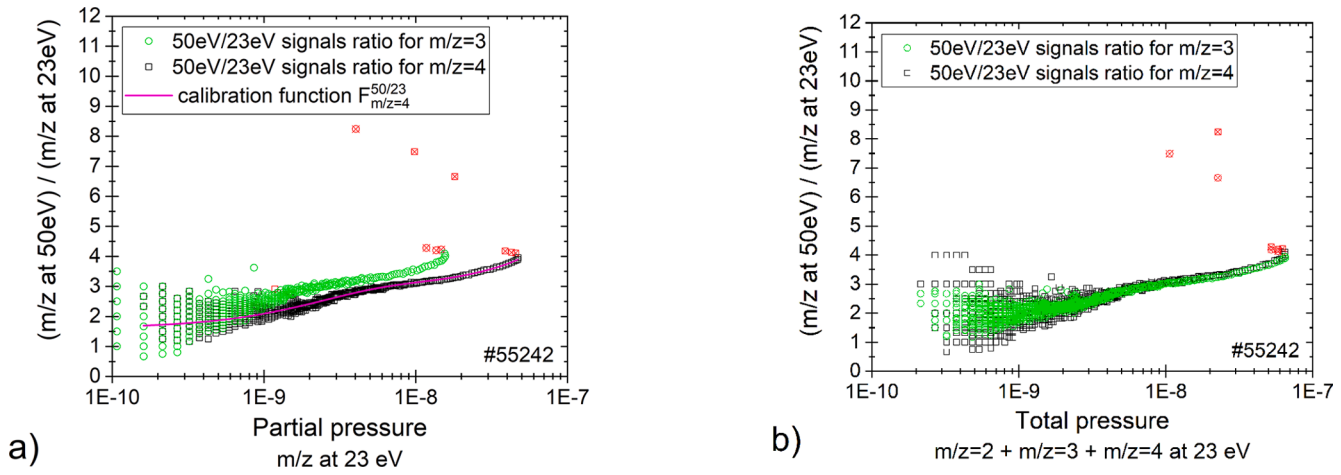

Fig. 2. Evolution of the ratio of signals measured at 50 eV and 23 eV, for $m/z = 3$ and $m/z = 4$, as a function of partial pressure (a) and as a function of total pressure (b) for the reference D discharge #55242. The calibration function $F^{50/23}_{m/z=4}$ for evaluating D_2 at 50 eV from D_2 measured at 23 eV is adjusted as a function of the partial pressure on the signal $m/z = 4$ (a). Crossed red symbols are not used in the calibration function adjustment and are related to rapidly changing pressure at plasma breakdown and plasma termination. (For interpretation of the references to colour in this figure legend, the reader is referred to the web version of this article.)

the origin of the variation of the calibration functions with pressure is related to the ionization head of the mass spectrometer, where all species are ionized, rather than to its mass filter or its electrometer where only mass-over-charge selected ions are located. Consistent with this interpretation, we observed that switching the ionization filament of the QMS changes significantly the calibration function $F^{50/23}_{m/z=4}$ and its evolution with partial pressure ($F^{50/23}_{m/z=4}$ varies between 6 and 7 with the second filament). However, it is not possible to use a calibration function defined as a function of total pressure since, during the D-to-He changeover campaign, the total pressure cannot be determined with the QMS because He and D_2 have different ionization cross sections and their balance in the outgassing flux is unknown *a priori*. Nevertheless, the use of the calibration functions $F^{50/23}_{m/z=4}$ and $F^{50/23}_{m/z=3}$, defined as a function of partial pressures, should be good approximations as long as the HD/D_2 isotopologues ratio remains relatively constant. We analyzed the first 110 s of all post-discharges reported here, excluding a 3 s "dead-time" explained in the next section, and found that the isotope ratio H/(H + D) for HD/D_2 species in the post-discharge is 27 ± 8% throughout the presented experimental campaign, granting the use of $F^{50/23}_{m/z=3} = 1.17 \times F^{50/23}_{m/z=4}$.

Finally, we evaluated the uncertainty coming from the use of calibration functions defined on partial pressures by calculating the relative difference between the measured HD partial pressure $P^{50eV}_{m/z=3}$ and the evaluated HD partial pressure $P^{23eV}_{m/z=3} \times F^{50/23}_{m/z=3}$ during the D reference discharge #55242. We found that the relative error originating from the calibration function remains within ± 5% in the first 100 s after plasma termination.

2.3. TIMS during tokamak operation: Calibration drifts and limitation from rapidly changing pressure

We also used the calibration function $F^{50/23}_{m/z=3}$ determined for $m/z = 3$ to check for the stability of the calibration along the WEST He changeover campaign. We found that the response of the QMS signal drifts in a systematic manner depending on the species used for the plasma discharge. This observation was realized by plotting for each discharge the $m/z = 3$ signal at 50 eV together with its evaluation from the signal at 23 eV using $F^{50/23}_{m/z=3}$. As analyzed and shown in Fig. 3, it was found that $F^{50/23}_{m/z=3}$ was gradually reduced by a constant factor as the He plasma discharges accumulated. Then the calibration function came back slowly close to its initial value as D plasma discharges were performed. Finally, the calibration function was reduced again when resuming He plasma discharges. We suggest that the apparent reversibility of the calibration function variation upon plasma species could be a chemical effect. Indeed, deuterium is a chemically reducing species and it might remove contaminants such as oxygen or carbon from the ionization head elements thereby changing the filament emission and/or modifying actual electrical potentials on ion extraction electrostatic lenses. Independently of the origin of this variation in the calibration function, we were able to use this systematic analysis of the drifts of the calibration function $F^{50/23}_{m/z=3}$ to counteract them for the evaluation of the He/D gas balance using $F^{50/23}_{m/z=4}$. For each plasma discharge, $F^{50/23}_{m/z=3}$ gives a correction factor (≤ 1 as shown in Fig. 3) with respect to the reference discharge #55242. By multiplying $F^{50/23}_{m/z=4}$ with this correction factor determined from $m/z = 3$, one obtains a He (and a D) gas balance that always fit nicely in the 0–100% range. The results presented in the next section include this drift correction.

Finally, Fig. 2a shows that the adjustment of the non-linear calibration function of the QMS response deviates from the actual response when reaching the highest partial pressures. In particular, one can see

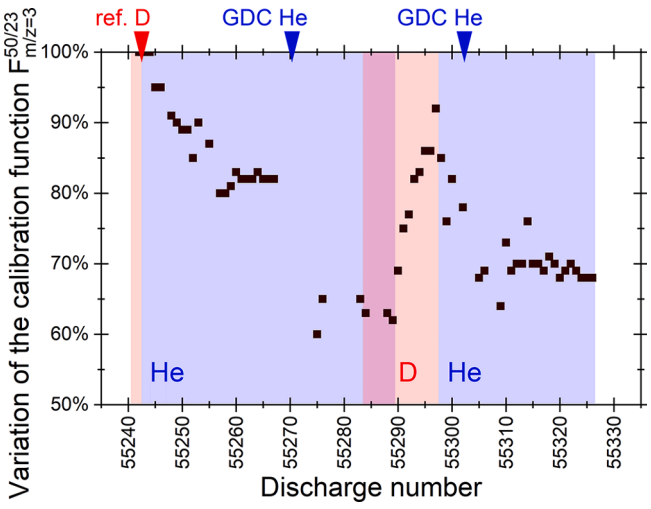

Fig. 3. Variation of the calibration function $F^{50/23}_{m/z=3}$ with respect to the reference D discharge #55242. This variation is sensitive to the species used for plasma discharge. The red areas indicate D discharges while the blue areas represent He discharges. The variation of $F^{50/23}_{m/z=3}$ with discharge number is used to correct $F^{50/23}_{m/z=4}$ allowing a He and D gas balance that always fit in the 0–100% range. (For interpretation of the references to colour in this figure legend, the reader is referred to the web version of this article.)

that $F^{50/23}_{m/z=3}$ and $F^{50/23}_{m/z=4}$ increase when increasing the QMS signal until they turn around and goes suddenly to high values for decreasing QMS signal (red crossed symbols in Fig. 2a and 2b). This odd behavior is related to rapidly changing pressures (on a time scale smaller than the sampling period of 0.685 s) by two orders magnitude during plasma breakdown and termination, respectively ranging from typically 10^{-5} Pa to 10^{-3} Pa. This can represent a limitation of TIMS during tokamak operation. In the current experiment, such pressure peaks create a "dead-time" for the accurate D/He gas balance estimation of about 2 s. This dead-time manifests itself as a He "ghost peak" whose amplitude is about 10% of the D_2 real signal (Fig. 4). We chose to not correct this He ghost peak in the present article but it may be accounted for in future studies.

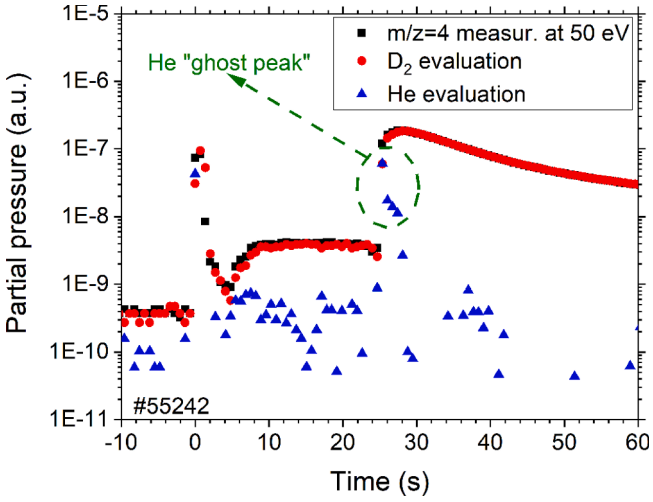

Fig. 4. In the reference D discharge used for calibration of the D_2 evaluation at 50 eV (#55242), a He "ghost peak" lasting about 2 s is erroneously evaluated just after the rapid pressure rise due to plasma termination (at a time of ~ 26 s). A similar ghost peak can be seen also at plasma breakdown around 0 s.

3. Results and discussion

3.1. Estimation of the uncertainty in measuring He and D traces during plasma discharges and post-discharges

As can be seen in Fig. 1, the typical pressure (although in arbitrary units) at the QMS during a discharge is about 100 times less than at the plasma termination. Thus, using a QMS with TIMS for determining a discharge gas balance containing species of identical masses is not a straightforward task. We found that in the best case (first He discharge #55243, with the highest pressure at the QMS of all He discharges), an absolute uncertainty of the order of ± 0.09 (evaluated as the standard deviation of the mean, ±σ) is obtained on the minority species (He) balance during the discharge (39%), i.e. a 25% relative uncertainty. However, the uncertainty rises quite rapidly as the pressure at the QMS decreases with the absolute uncertainty doubling when the pressure decreases by a factor of five in the present conditions i.e. relative uncertainties on the minority species (e.g. D_2 in #55250) become higher than 50%. Thus, TIMS appears to not be an adequate method for gas balance during plasma discharge, except close to the divertor region where large gas recycling occurs at plasma facing components such that sufficient pressure rise is obtained in the area where gases are sampled for QMS detection.

Regarding the post-discharge, absolute uncertainties are substantially reduced given the more favorable pressure conditions for applying TIMS following plasma termination. As shown in Fig. 5, for the first ten of He discharges we measured an absolute uncertainty on the D balance five seconds after the termination of the discharge comprised in the range ofσ_{5s} = 0.01–0.06 corresponding to the range of relative uncertainties 1–17%. Fifty seconds in the post-discharge the absolute uncertainties are within σ_{50s} = 0.01–0.06 corresponding to the range of relative uncertainties 1–6%. After 30 discharges and an overnight He GDC of four hours, the range of relative uncertainties on the D balance is still within 1–20% as long as the D absolute balance is above 5%. Only after about 50 discharges and 2 four hours He GDCs vessel conditioning, the QMS signal for $m/z = 4$ at 23 eV becomes weak and relative uncertainties on the D balance are above 20% fifty seconds after the termination of the discharge. Thus, in the present WEST He changeover campaign, TIMS is sufficiently sensitive to study systematically the effect of He plasma onto the relative gas balance of D and He species originating from tungsten plasma facing components.

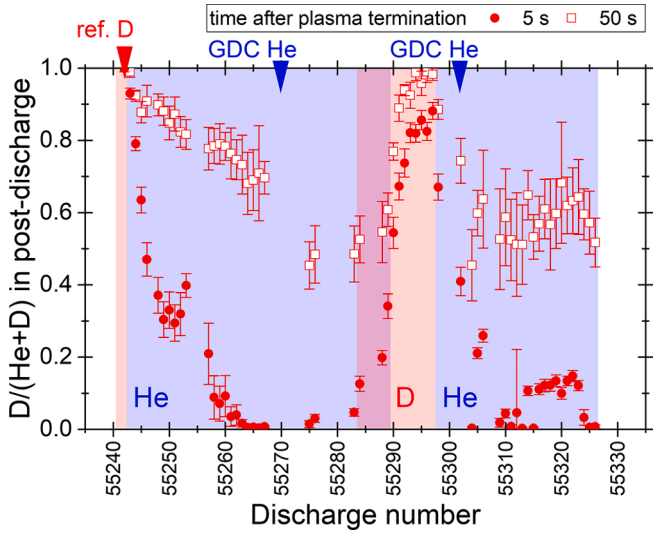

Fig. 5. Deuterium gas balance as a function of the discharge number determined at two different times after the plasma termination: 5 s (red solid circles) and 50 s (red open squares). The red areas indicate D discharges while the blue areas represent He discharges. (For interpretation of the references to colour in this figure legend, the reader is referred to the web version of this article.)

3.2. First observation of different outgassing behaviors for He and D in a full-W tokamak

In Fig. 5 we present the D gas balance along the He changeover campaign in the post-discharge, at two different times after plasma termination, 5 s and 50 s. Fig. 5 shows that it takes about 20 He discharges to remove D from the beginning (5 s) of the post-discharge. However, Fig. 5 shows also that, although only 9 D discharges were run during this period, after 74 He discharges and 2 overnights He GDCs there is still about 50% of D in the outgassing flux 50 s after the termination of the discharge. This observation results from two main differences in the He and D outgassing behavior in a full-W tokamak, as demonstrated in the following. The first difference is illustrated in Fig. 6a which shows the He/D balance for a disrupted He ohmic discharge (#55253, 0.5 MA current), i.e. a discharge abruptly terminated because of an uncontrolled loss of confinement. One can observe that in this case the He outgassing decays within 60 s down to the detection limit. However, the D outgassing decay is at least ten times slower with more than 600 s needed to reach detection limit, even though the initial pressure rise for D species was smaller than that for He. The second difference is illustrated in Fig. 6b that presents the He/D balance for a He ohmic discharge (#55257, 0.5 MA current) with a controlled quiescent termination. In addition to the same slower decay for D species than for He, one observes that the D species maximum outgassing is delayed by about 11 s from the plasma termination while He maximum outgassing occurs at plasma termination. The comparison of these two discharges ending either by an abrupt disruption or with a quiescent "landing" shows that the time behavior of the He outgassing is the same. However, the observation of a delayed D fuel outgassing for a quiescent termination, representing 20 times the QMS sampling rate, is striking. Such delayed outgassing may be explained by at least two mechanisms. Either D retention occurs deeper than He in the bulk of plasma facing components (and co-deposited layers) and thus D is outgassed later than He because of a longer particle diffusion in the bulk; or D retention and subsequent outgassing may occur in area away from the strike point region because of thermal diffusion.

3.3. Investigation of the origin of a delayed D outgassing during the D-to-He changeover campaign

In order to better pinpoint the origin of the delayed outgassing for D following the quiescent termination of a He discharge, we analyzed the evolution of the time delay for reaching the maximum D outgassing (Fig. 7) as well as the evolution of the maximum D outgassing flux (Fig. 8) for the first 60 discharges of the He changeover campaign. In these 60 discharges, about 40 were abruptly terminated (so called "disrupted") and about 20 had a quiescent termination and each termination type is populated with ohmic and Lower Hybrid (LH) current drive discharges. First, Fig. 7 shows that D outgassing is delayed by 10 s or more only for quiescent He plasma terminations, i.e. not disrupted, independently of the heating scheme (ohmic or LH) and this delay can be as large as 40 s. Second, Fig. 8 shows that the maximum D outgassing flux is decreasing almost monotonously on several orders of magnitude with increasing the discharge number.

The characteristic of a quiescent discharge termination is to keep the exhaust power located in the vicinity of the strike points on the divertor plasma facing components where most of the plasma wall interaction (recycling region) occurs during the discharge. In contrast, for a disrupted discharge the loss of confinement induces simultaneous thermal loads on many plasma facing components out of the strike point regions. Thus, on one hand, the immediate D outgassing for disrupted discharges can be understood as the results of simultaneous thermal loads on many plasma facing components far from the strike points that consequently outgassed in synchrony. On the other hand, the increasingly delayed D

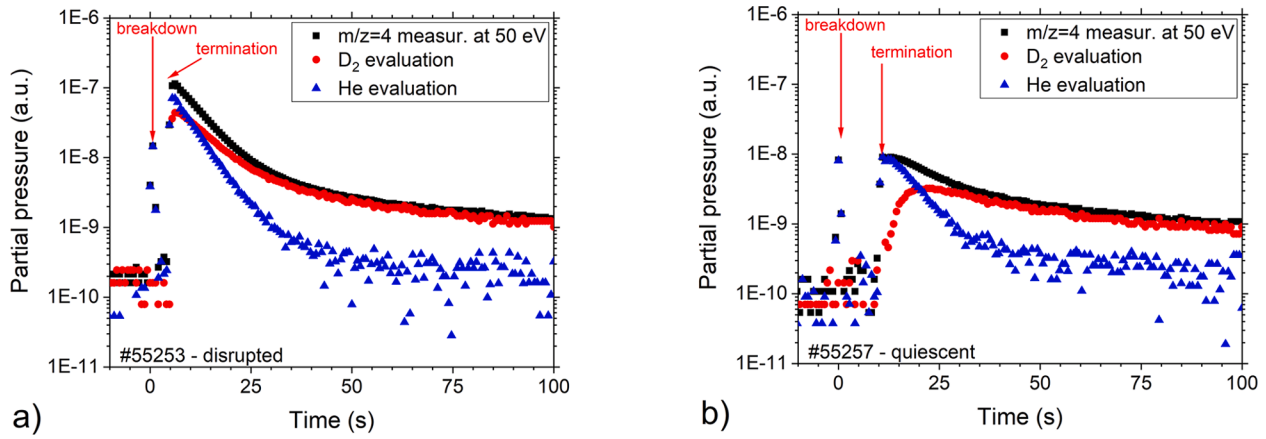

Fig. 6. He and D_2 evaluation in the post-discharge of two ohmic discharges (0.5 MA current), one being disrupted (a) and the other having a quiescent termination (b).

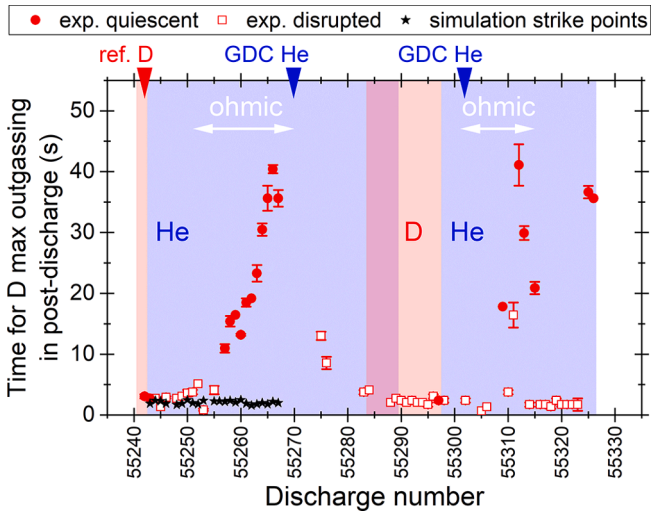

Fig. 7. Time delay at which the maximum of D outgassing is measured after plasma termination as a function of discharge number. The red areas indicate D discharges while the blue areas represent He discharges. Ohmic discharges are indicated within white arrows while other discharges are Lower Hybrid current drive discharges. Quiescent discharge terminations are represented by red solid circles. Disrupted discharges are indicated by red open squares. MHIMS simulations of the D outgassing of the strike points are shown by black stars. (For interpretation of the references to colour in this figure legend, the reader is referred to the web version of this article.)

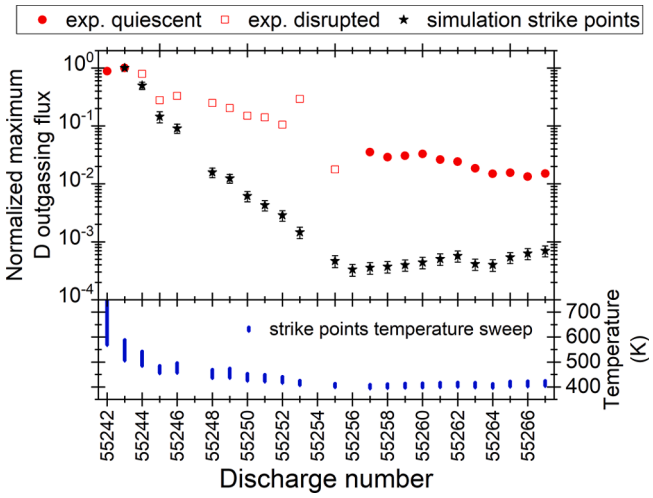

Fig. 8. Higher panel: maximum D outgassing flux measured after plasma termination as a function of discharge number (normalized to the maximum D outgassing flux of the first He discharge #55243). Quiescent discharge terminations are represented by red solid circles. Disrupted discharges are indicated by red open squares. MHIMS simulations of the strike points D outgassing are shown by black stars. Lower panel: extent of the temperature sweep experienced by the strike points (blue bar) as measured by thermocouples embedded in W-coated divertor plasma facing components. (For interpretation of the references to colour in this figure legend, the reader is referred to the web version of this article.)

outgassing observed for successive quiescent discharge terminations could be related to two different mechanisms: a D outgassing occurring mainly in (remote) areas away from the strike points i.e. the delay is related to thermal diffusion across plasma facing components; or a D outgassing from the strike points that gradually originates from deeper in the materials' bulk. In order to identify which of these two interpretations explains the observed delayed D outgassing for quiescent plasma terminations, we simulated the D outgassing from the divertor strike points with the following setup.

A Macroscopic Rate Equation (MRE) model implemented in the code MHIMS [19] is used to calculate the deuterium outgassing flux from the W divertor strike points. The divertor material is simulated as a 15 μm thick slab (corresponding to the thickness of the W coating on inertial graphite divertor plasma facing components). On the plasma facing side, a Dirichlet boundary condition (BC) is applied for the diffusive (mobile) deuterium, $c_m = 0$ i.e. the desorption of D arriving at the surface is instantaneous. On the opposite side, a Neumann BC is considered for the diffusive particles $\frac{\partial c_m}{\partial x} = 0$ to prevent desorption from the graphite substrate side. The energetics determining the trapping, the detrapping and the diffusion of D in W are taken from the literature at the level of the Density Functional Theory (DFT), since recent laboratory experiments on polycrystalline and single crystal tungsten have been successfully reproduced with such MRE-DFT setups [20,21]. The diffusion coefficient of D in W is calculated from Fernandez *et al.* energetics [22], while the energetics of bulk defect D trapping sites (eventually with co-trapped He) are taken from Bakaev *et al.* [23]. Detrapping energies $E_{dt,i}$ are calculated by adding the energy barrier for the diffusion (0.2 eV) to the binding energies calculated by Bakaev *et al.* Five different D trapping sites are considered and summarized in Table 1. The two grain boundaries traps have a high and constant homogeneous density in order to describe the microstructure expected from the W coating. These two traps are where the deuterium from the D reference discharge #55242 will initially trap. Then, three additional traps are used, He decorated vacancies, screw and edge dislocations, to describe the effect of He

Table 1
Summary of the defect trap types that are used in the simulation of D outgassing from tungsten divertor strike points during He discharges and post-discharges. Detrapping energies and (maximum) density used in the MRE-DFT model are indicated together with a comment about the time evolution and spatial distribution of the trap densities.

Defect	$E_{dt,i}$(eV)	n_i(at. fr.)	Defect density
Grain boundary Σ3 ⟨1 1 0⟩ {1 1 1}	1.3	10^{-3}	constant and homogeneous
Grain boundary Σ3 ⟨1 1 0⟩ {1 1 2}	0.85	10^{-3}	constant and homogeneous
Vacancy + He	1.2	5×10^{-3} (max)	varying at the subsurface
Screw dislocation + He	1.0	10^{-2} (max)	varying at the subsurface
Edge dislocation + He	1.3	10^{-2} (max)	varying at the subsurface

implantation on the W microstructure and the corresponding additional D trapping and detrapping in presence of He. These He-decorated defects are located in the first 100 nm of the bulk (subsurface), as it has been observed following stellarator He discharges as well as linear plasma He exposure [11,24]. Furthermore, the He-decorated defects densities increase with successive He discharges, as it has been observed with ion beam experiments [25], thanks to the trap creation model recently implemented in MHIMS [26].

The W divertor strike points simulation is initiated, either with a bulk free of deuterium or with a bulk full of deuterium (i.e. D is located at the grain boundaries). These two different initializations are used to determine the error bars interval of D outgassing flux shown in Fig. 8. The D reference discharge #55242 is simulated with a deuterium impinging flux of 10^{22} D.m^{-2}.s^{-1} at 50 eV/D. Then, the He discharges from #55243 to #55267 are simulated with the trap creation model. D outgassing during the whole #55242-#55267 discharge (and post-discharge) series are simulated using temperature measurements performed at the strike points area in WEST. The maxima of D outgassing are dictated by the temperature sweeps experienced by the W divertor strike points because of the thermal loads of D and He discharges, indeed. Thus, we used WEST embedded thermocouples in inertial W-coated plasma facing components to estimate the surface temperature at the strike points [27] during the discharge and post-discharge series and feed this thermal information in the MHIMS code. Eight of the twenty thermocouples (4 in the inner strike points area and 4 in the outer strike points area) are used to run separate MHIMS simulations. The D outgassing from these 8 simulations are summed up to have an estimation of the total D outgassing from strike points of the W-coated divertor plasma facing components in the He post-discharge. To ease the comparison, the outgassing flux evolution of the simulation and the experimental campaign are normalized to the results obtained for the first He discharge #55243.

Fig. 7 shows that the simulated delay in D outgassing at the strike points is 2 ± 0.5 s, independently of the plasma termination type. This simulated delay corresponds to the delay observed for the first He discharge #55243, which has a quiescent termination on the strike points. The simulated D outgassing delay also matches the ones observed for disrupted He discharges where various areas of plasma facing components are heated simultaneously because of the uncontrolled termination. However, the simulated D outgassing of the strike points fails to reproduce the increased delay observed for the later successive quiescent termination. This discrepancy can be understood by comparison of the simulated and experimental D outgassing flux. Fig. 8 shows that the simulated D outgassing flux from the strike points decreases by almost 4 orders of magnitude as the He discharges accumulate. In stark contrast, the experimental D outgassing flux decreased only by 2 orders of magnitude between the He discharges #55243 and #55267. The fact that experimental outgassing flux for the second quiescent discharges and the next ones are 1 to 2 orders of magnitude higher than the simulated strike points outgassing flux demonstrates that not only the striking points are outgassing but also other areas of the divertor during quiescent discharges. Thus, Fig. 8 shows that D outgassing from remote areas become rapidly predominant. Since Fig. 7 shows that modeled strike points D outgassing cannot reproduce the delay observed experimentally for successive quiescent discharges termination, we conclude that the observed delayed outgassing for quiescent plasma terminations is a signature of remote areas being slowly heated by thermal diffusion. Therefore, inertially-cooled W-coated components and/or deposition area should be culprits that explain the delayed D outgassing observed for quiescent He plasma terminations.

4. Conclusions

In the present study, we took advantage of the He changeover campaign in WEST to perform the first D/He gas balance during ohmic and LH discharges in a full-W tokamak using TIMS. A new calibration method for TIMS has been tested and the "operational domain" of TIMS during a real tokamak operation has been highlighted. The use of the ubiquitous HD isotopologue during a D discharge has been proposed to correct some shortcomings observed with the mass spectrometer used in TIMS measurements. Future application of TIMS could improve the time resolution of the method. With the present mass spectrometer configuration, a time resolution of less than 350 ms could be obtained if one would limit the TIMS measurements to the HD, D_2 and He species. Such improved time resolution could help to find ways to correct the dead-time of ca. 2 s of the TIMS method related to the rapidly changing pressure at plasma breakdown and plasma termination.

The TIMS analysis of the WEST He changeover campaign highlighted several differences in outgassing behavior for the He and D species during the post-discharge. First, the D species are outgassed for duration 10 times longer than for He. Second, the D species outgassing maximum can be delayed by tens of seconds with respect to plasma termination and He maximum outgassing if the plasma does not disrupt. The latter behavior has been seen for both ohmic and LH heating schemes. By comparing the experimental observations with a macroscopic rate equation model describing D outgassing from the divertor strike points, we interpret the delayed outgassing of D as the signature of thermal diffusion across inertially-cooled plasma facing components and/or thermally weakly coupled deposition area. It would be interesting to probe how the intensity of the delayed D outgassing will evolve when more actively-cooled W units will be installed in the WEST tokamak. These evolutions may help to better understand the role of deposition area in the dynamic retention and outgassing of fusion fuel in tokamaks.

Declaration of Competing Interest

The authors declare that they have no known competing financial interests or personal relationships that could have appeared to influence the work reported in this paper.

Acknowledgements

This work has been carried out within the framework of the French Federation for Magnetic Fusion Studies (FR-FCM) and of the EUROfusion Consortium and has received funding from the Euratom research and training programme 2014-2018 and 2019-2020 under grant agreement No 633053. The views and opinions expressed herein do not necessarily reflect those of the European Commission.

The project leading to this publication has also received funding from the Excellence Initiative of Aix-Marseille University – A*Midex, a French "Investissements d'Avenir" programme as well as from the ANR under grant ANR-18-CE05-12.

References

[1] ITER Organization, ITER Research Plan within the Staged Approach, 2018. https://www.iter.org/technical-reports?id=9 (accessed July 31, 2020).

[2] C.C. Klepper, T.M. Biewer, U. Kruezi, S. Vartanian, D. Douai, D.L. Hillis, C. Marcus, Extending helium partial pressure measurement technology to JET DTE2 and ITER, Rev. Sci. Instrum. 87 (11) (2016) 11D442, https://doi.org/10.1063/1.4963713.

[3] T. Coyne, N. Balshaw, D. Brennan, A. Miller, C. Whitehead, S. Davies, C. Robertson, De-convolution of complex residual gas spectra at JET, in: 2009 23rd IEEENPSS Symp. Fusion Eng., 2009: pp. 1–4. https://doi.org/10.1109/FUSION.2009.5226395.

[4] S. Davies, J.A. Rees, D.L. Seymour, Threshold ionisation mass spectrometry (TIMS); a complementary quantitative technique to conventional mass resolved mass spectrometry, Vacuum 101 (2014) 416–422, https://doi.org/10.1016/j.vacuum.2013.06.004.

[5] Yaowei Yu, Jiansheng Hu, Zhao Wan, Jinhua Wu, Houyin Wang, Bin Cao, Mass separation of deuterium and helium with conventional quadrupole mass spectrometer by using varied ionization energy, Rev. Sci. Instrum. 87 (3) (2016) 035120, https://doi.org/10.1063/1.4944560.

[6] C.C. Klepper, T.M. Biewer, C. Marcus, P. Andrew, W.L. Gardner, V.B. Graves, S. Hughes, Laboratory-based validation of the baseline sensors of the ITER diagnostic residual gas analyzer, J. Instrum. 12 (2017), https://doi.org/10.1088/1748-0221/12/10/C10012. C10012–C10012.

[7] C.C. Klepper, B. Pégourié, S. Vartanian, M. Goniche, E. Delabie, D. Van Eester, E. Lerche, G. Sips, I. Borodkina, D. Douai, I. Jepu, U. Kruezi, G.F. Matthews, A. Widdowson, Sub-divertor fuel isotopic content detection limit for JET and its impact on ICRF core heating and DTE2 operation, Nucl. Fusion 60 (1) (2020) 016021, https://doi.org/10.1088/1741-4326/ab4c5a.

[8] Shuang Cui, Michael Simmonds, Wenjing Qin, Feng Ren, George R. Tynan, Russell P. Doerner, Renkun Chen, Thermal conductivity reduction of tungsten plasma facing material due to helium plasma irradiation in PISCES using the improved 3-omega method, J. Nucl. Mater. 486 (2017) 267–273, https://doi.org/10.1016/j.jnucmat.2017.01.023.

[9] Suchandrima Das, Hongbing Yu, Edmund Tarleton, Felix Hofmann, Hardening and strain localisation in helium-ion-implanted tungsten, Sci. Rep. 9 (1) (2019), https://doi.org/10.1038/s41598-019-54753-3.

[10] M.J. Baldwin, R.P. Doerner, W.R. Wampler, D. Nishijima, T. Lynch, M. Miyamoto, Effect of He on D retention in W exposed to low-energy, high-fluence (D, He, Ar) mixture plasmas, Nucl. Fusion 51 (10) (2011) 103021, https://doi.org/10.1088/0029-5515/51/10/103021.

[11] Mykola Ialovega, Elodie Bernard, Régis Bisson, Celine Martin, Ryuichi Sakamoto, Arkadi Kreter, Etienne Hodille, Thierry Angot, Christian Grisolia, Hydrogen trapping in tungsten: impact of helium irradiation and thermal cycling, Phys. Scr. T171 (2020) 014066, https://doi.org/10.1088/1402-4896/ab68bd.

[12] G. De Temmerman, T. Hirai, R.A. Pitts, The influence of plasma-surface interaction on the performance of tungsten at the ITER divertor vertical targets, Plasma Phys. Control. Fusion 60 (4) (2018) 044018, https://doi.org/10.1088/1361-6587/aaaf62.

[13] J. Bucalossi, M. Missirlian, P. Moreau, F. Samaille, E. Tsitrone, D. van Houtte, T. Batal, C. Bourdelle, M. Chantant, Y. Corre, X. Courtois, L. Delpech, L. Doceul, D. Douai, H. Dougnac, F. Faïsse, C. Fenzi, F. Ferlay, M. Firdaouss, L. Gargiulo, P. Garin, C. Gil, A. Grosman, D. Guilhem, J. Gunn, C. Hernandez, D. Keller, S. Larroque, F. Leroux, M. Lipa, P. Lotte, A. Martinez, O. Meyer, F. Micolon, P. Mollard, E. Nardon, R. Nouailletas, A. Pilia, M. Richou, S. Salasca, J.-M. Travère, The WEST project: Testing ITER divertor high heat flux component technology in a steady state tokamak environment, Fusion Eng. Des. 89 (7-8) (2014) 907–912, https://doi.org/10.1016/j.fusengdes.2014.01.062.

[14] C. Bourdelle, J.F. Artaud, V. Basiuk, M. Bécoulet, S. Brémond, J. Bucalossi, H. Bufferand, G. Ciraolo, L. Colas, Y. Corre, X. Courtois, J. Decker, L. Delpech, P. Devynck, G. Dif-Pradalier, R.P. Doerner, D. Douai, R. Dumont, A. Ekedahl, N. Fedorczak, C. Fenzi, M. Firdaouss, J. Garcia, P. Ghendrih, C. Gil, G. Giruzzi, M. Goniche, C. Grisolia, A. Grosman, D. Guilhem, R. Guirlet, J. Gunn, P. Hennequin, J. Hillairet, T. Hoang, F. Imbeaux, I. Ivanova-Stanik, E. Joffrin, A. Kallenbach, J. Linke, T. Loarer, P. Lotte, P. Maget, Y. Marandet, M.L. Mayoral, O. Meyer, M. Missirlian, P. Mollard, P. Monier-Garbet, P. Moreau, E. Nardon, B. Pégourié, Y. Peysson, R. Sabot, F. Saint-Laurent, M. Schneider, J.M. Travère, E. Tsitrone, S. Vartanian, L. Vermare, M. Yoshida, R. Zagorski, WEST Physics Basis, Nucl. Fusion 55 (6) (2015) 063017, https://doi.org/10.1088/0029-5515/55/6/063017.

[15] Y.-K. Kim, K.K. Irikura, M.E. Rudd, M.A. Ali, P.M. Stone, J. Chang, J.S. Coursey, R. A. Dragoset, A.R. Kishore, K.J. Olsen, A.M. Sansonetti, G.G. Wiersma, D.S. Zucker, M.A. Zucker, Electron-Impact Cross Sections for Ionization and Excitation Database, 2004. dx.doi.org/10.18434/T4KK5C (accessed July 31, 2020).

[16] V. Kh Alimov, O.V. Ogorodnikova, Y. Hatano, YuM. Gasparyan, V.S. Efimov, M. Mayer, Z. Zhou, M. Oyaizu, K. Isobe, H. Nakamura, T. Hayashi, Surface modification and deuterium retention in reduced-activation steels exposed to low-energy, high-flux pure and helium-seeded deuterium plasmas, J. Nucl. Mater. 502 (2018) 1–8, https://doi.org/10.1016/j.jnucmat.2018.01.060.

[17] T. Loarer, T. Dittmar, E. Tsitrone, R. Bisson, C. Bourdelle, S. Brezinsek, J. B. Bucalossi, Y. Corre, L. Delpech, C. Desgranges, Long discharges in steady state with D2 and N2 on the actively cooled tungsten upper divertor in WEST, Nucl. Fusion. (2020), https://doi.org/10.1088/1741-4326/abb919.

[18] Donald Rapp, Paula Englander-Golden, Total Cross Sections for Ionization and Attachment in Gases by Electron Impact. I. Positive Ionization, J. Chem. Phys. 43 (5) (1965) 1464–1479, https://doi.org/10.1063/1.1696957.

[19] E.A. Hodille, X. Bonnin, R. Bisson, T. Angot, C.S. Becquart, J.M. Layet, C. Grisolia, Macroscopic rate equation modeling of trapping/detrapping of hydrogen isotopes in tungsten materials, J. Nucl. Mater. 467 (2015) 424–431, https://doi.org/10.1016/j.jnucmat.2015.06.041.

[20] E.A. Hodille, F. Ghiorghiu, Y. Addab, A. Založnik, M. Minissale, Z. Piazza, C. Martin, T. Angot, L. Gallais, M.-F. Barthe, C.S. Becquart, S. Markelj, J. Mougenot, C. Grisolia, R. Bisson, Retention and release of hydrogen isotopes in tungsten plasma-facing components: the role of grain boundaries and the native oxide layer from a joint experiment-simulation integrated approach, Nucl. Fusion 57 (7) (2017) 076019, https://doi.org/10.1088/1741-4326/aa6d24.

[21] F. Ghiorghiu, M. Minissale, E.A. Hodille, C. Grisolia, T. Angot, R. Bisson, Comparison of dynamic deuterium retention in single-crystal and poly-crystals of tungsten: The role of natural defects, Nucl. Instrum. Methods Phys. Res. Section B: Beam Interactions Mater. Atoms 461 (2019) 159–165, https://doi.org/10.1016/j.nimb.2019.09.032.

[22] N. Fernandez, Y. Ferro, D. Kato, Hydrogen diffusion and vacancies formation in tungsten: Density Functional Theory calculations and statistical models, Acta Materialia 94 (2015) 307–318, https://doi.org/10.1016/j.actamat.2015.04.052.

[23] Alexander Bakaev, Dmitry Terentyev, Evgeny E. Zhurkin, Ab initio study of the stability of H-He clusters at lattice defects in tungsten, Nucl. Instrum. Methods Phys. Res. Section B: Beam Interactions Mater. Atoms 478 (2020) 269–273, https://doi.org/10.1016/j.nimb.2020.06.033.

[24] E. Bernard, R. Sakamoto, N. Yoshida, H. Yamada, Temperature impact on W surface exposed to He plasma in LHD and its consequences for the material properties, J. Nucl. Mater. 463 (2015) 316–319, https://doi.org/10.1016/j.jnucmat.2014.11.041.

[25] H. Iwakiri, K. Yasunaga, K. Morishita, N. Yoshida, Microstructure evolution in tungsten during low-energy helium ion irradiation, J. Nucl. Mater. 283–287 (2000) 1134–1138, https://doi.org/10.1016/S0022-3115(00)00289-0. Part 2.

[26] E.A. Hodille, S. Markelj, T. Schwarz-Selinger, A. Založnik, M. Pečovnik, M. Kelemen, C. Grisolia, Stabilization of defects by the presence of hydrogen in tungsten: simultaneous W-ion damaging and D-atom exposure, Nucl. Fusion 59 (1) (2019) 016011, https://doi.org/10.1088/1741-4326/aaec97.

[27] J. Gaspar, Y. Corre, M. Firdaouss, J.L. Gardarein, J. Gerardin, J.P. Gunn, M. Houry, G. Laffont, T. Loarer, M. Missirlian, J. Morales, P. Moreau, C. Pocheau, E. Tsitrone, First heat flux estimation in the lower divertor of WEST with embedded thermal measurements, Fusion Eng. Des. 146 (2019) 757–760, https://doi.org/10.1016/j.fusengdes.2019.01.074.